# The optimum fire window: applying the fire-productivity hypothesis to Jurassic climate states

Teuntje P. Hollaar*[1,2], Claire M. Belcher[1], Micha Ruhl[3], Jean-François Deconinck[4], Stephen P. Hesselbo[2,5]

[1]WildFIRE Lab, Global Systems Institute, University of Exeter, Exeter, EX4 4PS, UK

[2]Camborne School of Mines, Department of Earth and Environmental Sciences, University of Exeter, Penryn Campus, Penryn, TR10 9FE, UK

[3]Department of Geology, Trinity College Dublin, The University of Dublin, College Green, Dublin, Ireland

[4]Biogéosciences, UMR 6282 CNRS, Université de Bourgogne/Franche-Comté, 21000 Dijon, France

[5]Environment and Sustainability Institute, University of Exeter, Penryn Campus, Penryn, TR10 9FE, UK

*Corresponding author: t.p.hollaar@uu.nl

**Abstract**

Present day fire frequency has been related to a productivity/aridity gradient on a regional and global scale. Optimum fire conditions occur at times of intermediate productivity and aridity, whereas fire is limited on the high productivity (moisture) and aridity (no fuel) endmembers. However, the current global fire activity pattern is reinforced by the predominant burning of grasslands. Here we test the intermediate fire-productivity hypothesis for a period on Earth before the evolution of grasses, the Early Jurassic, and explore the fire regime of two contrasting climatic states: the Late Pliensbachian (LPE) cooling Event and the Sinemurian–Pliensbachian Boundary (SPB) warming. Palaeo-fire records are reconstructed from fossil charcoal abundance, and changes in the hydrological cycle are tracked via clay mineralogy, which allows inference of changes in fuel moisture status. Large fluctuations in the fossil charcoal on an eccentricity time scale indicate two modes of fire regime at the time. Wildfires were moisture limited in a high productivity ecosystem during eccentricity minima for both the SPB and LPE. During eccentricity maxima, fires increased, and an optimum fire window was reached, in which greater seasonality in rainfall and temperatures led to intermediate states of productivity and aridity. The LPE experienced more extreme climatic endmembers compared to the SPB, with the fire regime edging closer to 'moisture limitation' during eccentricity minima, and more

pronounced seasonality during eccentricity maxima, explained by the overall cooler climate at the time. This study illustrates that the intermediate-productivity gradient holds up during two contrasting climatic states in the Jurassic.

**Plain Language Summary**

Fires are limited in year-round wet climates (tropical rainforests, too wet), and in year-round dry climates (deserts, no fuel). This concept, the intermediate-productivity gradient, explains the global pattern of fire activity. Here we test this concept for climate states of the Jurassic (~190 Myr ago). We find that the intermediate-productivity gradient also applies in the Jurassic, despite the very different ecosystem assemblages, with fires most frequent at times of high seasonality.

**Key Points**

- The intermediate-fire productivity gradient can be applied to the Jurassic and be utilized to explain changes in biomass abundance, moisture availability, and fire activity.
- The terrestrial ecosystem surrounding the Cardigan Bay Basin was not year-round dry during the Sinemurian–Pliensbachian Boundary warming Event or the Late Pliensbachian Cooling Event and therefore fire was not aridity limited.
- Fire activity was strongly influenced by the ~100 kyr and 405 kyr eccentricity cycle during both climatic states, which led to two modes in the fire regime: productivity limited (minima) and the optimum fire-window (maxima).

## 1 Introduction

The global distribution of fire at the present day follows the intermediate-productivity hypothesis. This hypothesis suggests that fire activity increases non-linearly along a productivity gradient primarily controlled by biomass and fuel availability (Pausas & Bradstock, 2007; Pausas & Ribeiro, 2013). Climate drives fuel availability, structure, and moisture, which are the main determinants of the fire regime. Where the fire regime reflects the frequency, behaviour, type of fire, and the impact on the ecosystem (Bradstock, 2010). Fire is either limited by high moisture in ecosystems with high biomass production, for example in tropical rainforests, or in high aridity and low biomass production ecosystems, with disconnected fuel such as in deserts. This principle explains drought-driven fire regimes and fuel-limited fire regimes (Pausas & Ribeiro, 2013). In humid regions fires are initiated by seasonal aridity which leads to flammable conditions and lower fuel-moisture status. Rising temperatures can lead to increased drought and flammability in high productivity ecosystems and further accelerate this drought-driven increase in fire activity (Pausas & Ribeiro, 2013). In unproductive arid regions it is biomass production that determines fire activity, as the fuel-moisture status would not be limiting (Pausas & Ribeiro, 2013). The optimum window for wildfires is at intermediate productivity levels, such as in the tropical savannahs of today, wherein biomass can accumulate due to seasonal precipitation and fuel becomes available in the dry season when the fuel moisture status decreases (Meyn et al., 2007; Pausas & Bradstock, 2007; Krawchuk & Moritz, 2011; Pausas & Paula, 2012; Pausas & Ribeiro, 2013).

The intermediate-productivity concept provides an effective explanation for the distribution of fire on a global and regional scale in the modern day where highest fire activity is found at intermediate moisture availability (Meyn et al., 2007; Krawchuk & Moritz, 2011; Daniau et al., 2012). The observation of high fire activity in ecosystems that are of intermediate aridity and productivity is strongly driven by grass biomes today (Archibald et al., 2018), where >80 % of area burnt is in grasslands (van der Werf et al., 2006). Although the intermediate-productivity gradient hypothesis of the present day is strongly linked to the expanse of grassland habitats, it should not require the presence of grasses to explain the impact of climate and seasonality on fire frequency in other vegetation types. The crucial concept is that an optimum fire window exists when there is a sufficiently moist season that allows fuel growth which is followed by a drier season in which fuel moisture levels are lowered, allowing ignition and fire spread. Since fire has formed an important part of ecosystems and the Earth system since 420 Ma (Glasspool et al., 2004; Glasspool & Gastaldo, 2022), we therefore test whether the intermediate-productivity gradient has also existed and if the concept can also be applied in a world before the evolution of grasses.

Here we look back at two contrasting climate events in the Early Jurassic, ~190 Myr ago, to assess what evidence there is for the existence of the intermediate-productivity fire gradient at such time

100 (Fig. 1). The first event, the Sinemurian-Pliensbachian Boundary event (SPB, is marked by global

101 warming, sea-level rise, increased humidity, and a negative carbon-isotope excursion (Ruhl et al.,

102 2016; Haq, 2018; Deconinck et al., 2019; Storm et al., 2020). In contrast, the second event, the late

103 Pliensbachian Event (LPE) is marked by ~5 °C cooling in NW Europe, greater aridity, sea-level fall

104 and a global positive carbon-isotope excursion (e.g. Korte et al., 2015; Ruhl et al., 2016; Haq, 2018;

105 Deconinck et al., 2019; Storm et al., 2020). We couple charcoal, clay and climate data to infer palaeo-

106 fire and the hydrological regimes during both these time intervals.

107

108 2 Materials and Methods

109 Materials

110 The records from both the LPE and SPB are taken from the Llanbedr (Mochras Farm) borehole, from

111 sedimentary strata deposited in a relatively deep marine setting close to the shore in the Cardigan Bay

112 Basin (Wales, UK). These sediments show a strong regular orbital control in the limestone-mudstone

113 alternations (Ruhl et al., 2016), and an existing astrochronological framework provides an age model

114 for the Mochras borehole. In addition, input of terrestrial organic matter in the sampled section is

115 relatively high (van de Schootbrugge et al., 2005; Riding et al., 2013), and thus provides ideal

116 material to study palaeo-fire regimes with a relatively high temporal constraint.

117
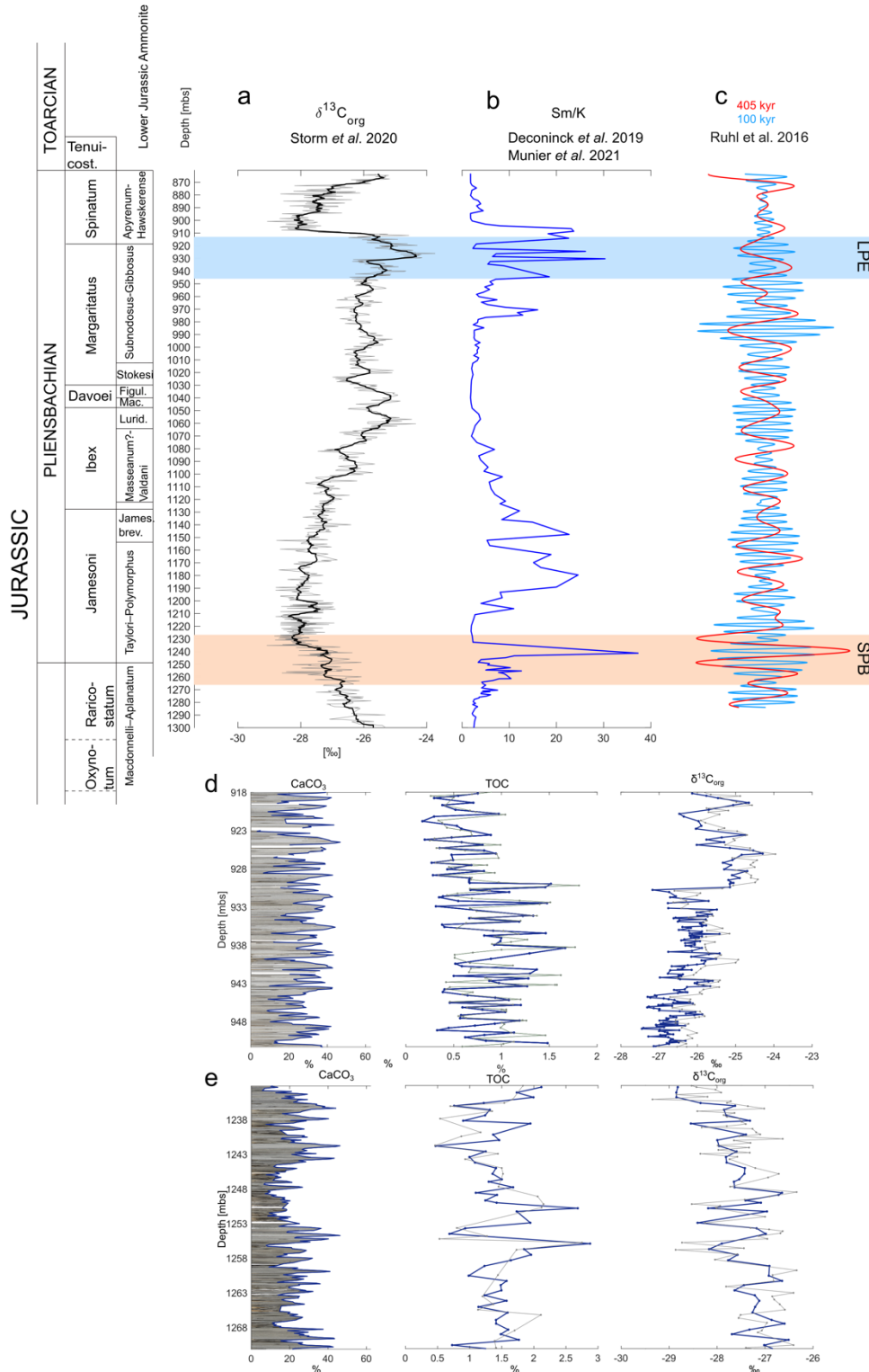
**Fig. 1:** *Cyclostratigraphic framework of the latest Sinemurian–Pliensbachian of the Mochras core and the two intervals here studied. Red bar represents the interval (1271–1233 metres below surface (mbs)) of the SPB and the blue bar represents the interval of the LPE (951–918 mbs) (a) The $\delta^{13}C_{org}$ record from the Mochras core (Storm et al., 2020), shows the broad negative carbon-isotope trend around the SPB and the positive carbon-isotope excursion (CIE) in the Late Pliensbachian. (b) The*

*smectite/kaolinite (Sm/K) ratio reflects changes in the hydrological cycle; data from Deconinck et al.*

*(2019) and Munier et al. (2021). Peaks in smectite indicate greater climatic aridity (Deconinck et al.,*

*2019; Munier et al., 2021). (c) The bandpass-filtered Ca-elemental record in the depth domain from*

*Ruhl et al. (2016) representing the 100 kyr and 405 kyr cycle. (d) The LPE interval is carbonate-rich*

*and shows the metre-scale variations in $CaCO_3$ and TOC, next to the $\delta^{13}C_{org}$ positive shifts that marks*

*the onset of the LPE. (e) The SPB interval contains relatively more clay and lithological couplets of*

*alternating $CaCO_3$ and TOC-enhanced beds occurring on a metre scale. The $\delta^{13}C_{org}$ shows the*

*negative trend of the long-negative limb of the SPB negative CIE.*

The Mochras core was drilled between 1967 and 1969 on the coast in NW Wales, UK. Preserved 1-m-length core slabs of the core are stored at the British Geological Survey National Core Repository at Keyworth, United Kingdom. The Pliensbachian of Mochras shows alternating beds of pale grey limestone and dark brown to grey mudstone (Ruhl et al., 2016). These couplets occur throughout the Pliensbachian, but vary in thickness, from about 90 cm at the Sinemurian–Pliensbachian boundary to about 30 cm in the Late Pliensbachian age strata (latest Margaritatus and Spinatum zones) (Ruhl et al., 2016). The lithological couplets are well expressed around the SPB and in the Margaritatus Zone (Ruhl et al., 2016). For this study, samples were taken at an average sample spacing of 90 cm across the Sinemurian–Pliensbachian boundary (1272–1233 mbs (metres below surface)). In addition, data are utilized in this study that are published in Hollaar et al. (2021; 2023), from the Late Pliensbachian interval that is sampled at a 10 cm (951–934 mbs) and 30 cm (934–918 mbs) resolutions. The macrocharcoal data between 934–918 mbs are new and not previously published. An overview of the number of samples per stratigraphic interval and proxy can be found in SI Table 1.

*Palaeolocation and provenance*

During the Early Jurassic, the Mochras site was situated in the Boreal realm of the Laurasian Seaway, which contained an island archipelago, and covers most of present-day NW and W Europe. The Mochras site was situated at a palaeolatitude of ~35° N (Torsvik & Cocks, 2017), just off the Welsh Massif, in a relatively deep marine setting, below storm base (Pieńkowski et al., 2021), but with a strong terrestrial influence (van de Schootbrugge et al., 2005; Riding et al., 2013; Xu et al., 2018; Storm et al., 2020).

The Welsh Massif was likely the main detrital source to the Cardigan Bay Basin (Deconinck et al., 2019), although other emergent areas in proximity likely also contributed (Deconinck et al., 2019). The nearby Irish Massif, situated west of the Welsh Massif, also cannot be dismissed as a source of nutrients, terrestrial organic particles, clay and coarser mineral grains to the Cardigan Bay Basin (Deconinck et al., 2019). Another possible source area is the emergent land of the Scottish Massif to the north of the Mochras Borehole and the London-Brabant Massif to the east of the Mochras Borehole (van de Schootbrugge et al., 2005).

158    The multiple nearby landmasses contributing runoff to the here studied relatively deeper marine

159    depositional environment, allowed for the charcoal record presented in this study to reflect a regional

160    expression of likely multiple fires. These fires might have in part occurred synchronous, but it is also

161    important to note that one stratigraphic rock sample in this study represents a ~2 kyr average signal,

162    which likely is more than the fire return interval at the time of deposition and thus represents an

163    averaging of the overall fire signal through time and space. Therefore, the term 'fire activity' here

164    describes the overall occurrences as increases and decreases in wildfires across the region.

165    In this study we measure the abundance of microcharcoal and macrocharcoal as a proxy for fire

166    activity. The size of charcoal fragments is often used as an indicator if the fires were proximal or

167    distal to the deposition site. Often larger more proximal charcoal particles are found in terrestrial

168    biomes and their depositional environments, in soils, lakes and mires. In contrast, smaller charcoal

169    particles that are wind-blown could potentially end up in a marine environment, as well as in more

170    distal terrestrial settings. However, experimental research showed that riverine transport has the

171    potential to carry the larger charcoal particles further away from shore, with the smaller charcoal

172    particles becoming water saturated at a shorter distance and settling down closer to the shoreline

173    (Nichols et al., 2000). In addition to this, other studies have indicated that larger charcoal particles (up

174    to 7 cm) can be windblown and travel up to 50 km from the original source, depending mainly on

175    their morphology (Woodward & Haines, 2020). Combined, charcoal size, shape, properties, wind

176    direction, plume height, but also riverine and marine transportation, all have a different impact on the

177    travel distance of different charcoal size classes. Hence, in the context of this study, no inferences can

178    be made about the different size classes and therefore microcharcoal and macrocharcoal both serve as

179    an overall indicator of fire activity.

180

181    *Methods*

182    Mass spectrometry $\delta^{13}C_{org}$, TOC and $CaCO_3$

183    Bulk organic carbon-isotopes, TOC and carbonate content were measured to track changes in the

184    carbon-cycle and changes in total organic matter in the studied interval. For the SPB interval (1271–

185    1233 mbs) 50 samples and for the LPE (918–951 mbs) 193 samples were processed for carbon

186    isotope mass spectrometry. Bulk rock samples were powdered using a pestle-a-mortar, weighed into

187    centrifuge tubes, and decarbonated using 3.3 % HCl. Following, the samples were transferred to a hot

188    bath (79 °C) for 1 h to remove siderite and dolomite. After this, the samples were centrifuged and the

189    liquid decanted, this step repeated until the samples were neutralized (on average 2 times). Finally, the

190    samples were oven-dried, re-powdered, and weighed (to measure $CaCO_3$ loss) and transferred into

191    small tin capsules for mass spectrometry (TOC and $\delta^{13}C_{org}$), at the University of Exeter, Penryn

192    Campus.

194    For the SPB interval, 54 samples were prepared for charcoal analysis and 42 for palynofacies at the

195    University of Exeter, Streatham Campus. For the LPE interval, an additional 50 macrocharcoal

196    samples were analysed, to compliment a total of 204 macrocharcoal samples for this interval. A total

197    of 162 samples for palynofacies and 200 microcharcoal samples are included in the LPE study

198    interval.

199    Rock samples of 10–30 g weight were split into 0.5 cm$^3$ fragments to minimize the breakage of the

200    organic particles whilst optimizing the surface area for palynological acid maceration. First, the 190

201    samples were treated with 10 % and 37 % HCl to remove carbonate. After this, hydrofluoric acid (40

202    % HF) was added to remove silicates from the sample. The samples were left to digest for 48 h, after

203    which cold concentrated HCl (37 %) was added to avoid calcium fluoride precipitation. Each sample

204    was left to settle, after which it could be decanted and topped up with DI water, a step that was

205    repeated ~6 times in order for the sample to neutralize.

206    After neutralizing, 5 droplets of the mixed residue were taken for the analysis of palynofacies (total

207    particulate organic matter) prior to any sieving. The remaining residue was sieved through a 125 μm

208    sieve and a 10 μm sieve to retrieve the macroscopic fraction (> 125 μm) and microscopic fraction

209    (10–125 μm). Macroscopic charcoal (>125 μm) was quantified using a Zeiss Stemi microscope, with

210    a 10 x 4 magnification lens and top lighting from a 'goose necked' light source. The entire

211    macroscopic fraction was dispersed in a Petri dish filled with DI water and the number of charcoal

212    particles counted and expressed per 10 g of processed rock (n/g). In some samples large clusters of

213    matrix were not digested by the acid, in which case they were taken out and dry weighed to deduce

214    the weight of the total processed rock. Charcoal particles are identified as opaque, black, angular,

215    reflective of light, with lustrous shine, elongated, lacking brown edges, and splintering during

216    breakage, and often showing the anatomical structure of the plant preserved (SI Fig. 1 and SI Table 2,

217    Scott, 2000; Scott & Damblon, 2010).

218    Microscopic charcoal (10–125 μm) was analysed on a palynological slide. A known quantity of 125

219    μl of the microscopic fraction was mounted onto microscopic slides using glycerine jelly. A

220    transmitted light microscope (Olympus (BX53)) with a 40 x 10 magnification was used to count the

221    charcoal particles. Four transects per slide were counted, one transect on the left, two in the middle,

222    and one on the right of the coverslip. These data were then scaled up to the known quantity of the total

223    sample (Belcher et al., 2005). Palynofacies were examined to record shifts in the type of organic

224    matter (terrestrial vs marine) and potential changes in organic matter preservation and/or terrestrial

225    runoff. Palynofacies were quantified using the optical light microscope and a minimum of 300 organic

226    particles per palynological slide was counted. The types of organic matter were roughly grouped after

227    Oboh-Ikuenobe et al. (2005): terrestrial palynomorphs (spores and pollen), marine palynomorphs

(dinoflagellates, acritarchs, prasinophytes and foraminifera test linings), fungal remains, structured phytoclasts (wood particles, parenchyma), unstructured phytoclasts (degraded plant remains), charcoal, black debris (palynomorphs filled with pyrite) and amorphous organic matter (AOM: fluffy, clotted and granular masses, colour ranging between almost colourless to yellow and pale brown).

## XRD clay mineralogy

A total of 55 samples were prepared for clay mineralogy spanning the SPB interval and 194 samples for the LPE interval. About 5 g of bulk-rock sample was gently crushed and powdered with an agate mortar, after which about 2–3 g of the powdered sample was decarbonated with a 0.2 M HCl solution. The samples were left to settle for 95 min, after which the suspended clay sized fraction (< 2 μm) was extracted with a syringe (following Stokes' law). The clay fraction was centrifuged and subsequently smeared and oriented on glass slides. The samples were analysed by X-ray diffraction (XRD) using a Bruker D4 Endeavour diffractometer (Bruker, Billerica, MA, USA) with Cu Kα radiations, LynxEye detector and Ni filter under 40 kV voltage and 25 mA intensity at the Biogéosciences Laboratory, Université Bourgogne/FrancheComté, Dijon. Three runs were performed per sample to discriminate the clay phases: (1) air-drying at room temperature; (2) ethylene-glycol solvation for 24 h; (3) heating at 490 °C for 2 h, following Moore & Reynolds (1997). Comparing the three diffractograms obtained, the clay minerals were identified using their main diffraction (d0001) peak. The proportions of each clay mineral on glycolated diffractograms was estimated with the MACDIFF 4.2.5 software (Petschick, 2000). The identification of the clay minerals further follows the methods in Moore & Reynolds (1997) and Deconinck et al. (2019).

## Statistical analysis

## Orbital filters and the charcoal record

The Pliensbachian of the Mochras core has a well-established astrochronological framework (Ruhl et al., 2016; Hinnov et al., 2018; Storm et al., 2020; Hollaar et al., 2021; Pienkowski et al., 2021). Based on the existing cyclostratigraphy, the 100 kyr eccentricity cycle lies within the range of 3.2–10.2 m (Ruhl et al., 2016; Hinnov et al., 2018), 6.3–4.8 m (Storm et al., 2020), and ~5.3 m (Pieńkowski et al., 2021) for the here studied SPB and LPE intervals. These intervals each compromise ~7–8 short eccentricity cycles. No spectral analysis has been performed on the records presented here because of the limited time span represented. Instead, we compare the charcoal and clay records visually with the 100 kyr and 405 kyr filters based on Ca and Ti (Ruhl et al., 2016; Hinnov et al., 2018). In SI Fig. 2 we overlay the 3.2 – 10 m filter (based on Ruhl et al., 2016) derived from the macrocharcoal record with the normalized dataset of the macrocharcoal record.

## Pearson correlation

A Pearson correlation was used to test for possible correlation between the charcoal abundance (both size fractions) and palynofacies and the significance using RMatlab2021b. The p value tests the

263    hypothesis of no correlation against the alternative hypothesize of a positive or negative correlation,

264    with the significance level at a = 0.05. See SI Fig. 3.

265    Wilcoxon test

266    A Wilcoxon rank sum test was performed in RMatlab2023b to test the null hypothesis of equal means

267    between the charcoal populations of the LPE and the SPB interval with the significance level at a =

268    0.05. The test is performed for the macrocharcoal and microcharcoal records separately.

269    PCA analysis

270    Principal component analysis (PCA) was performed to explore the potential covariance of charcoal,

271    clay mineralogy, palynofacies and mass-spectrometry records for the two studied intervals. This was

272    executed in the software PAST (Hammer et al., 2001) on the normalized dataset (macrocharcoal,

273    microcharcoal, TOC, $CaCO_3$, $\delta^{13}C_{org}$, S/I, Sm/K, K/I, phytoclasts).

274    **3 Results**

275    The data presented here that cover the run-up to and onset of the SPB (1271–1233 mbs) show a ~1.8

276    ‰ negative shift in $\delta^{13}C_{org}$ spanning the end of the negative CIE limb in the Mochras borehole and

277    reaching most negative values. The results of the LPE interval which encompass the run-up and onset

278    of the LPE (951 – 918 mbs), show a rapid positive shift in the $\delta^{13}C_{org}$ of ~1.8 ‰ (between 930.8 –

279    930.4 mbs) (in agreement with Storm et al., 2020).

280    Large fluctuations are observed in the abundance of both macroscopic (>125 μm) and microscopic

281    (10–125 μm) fossil charcoal for both CIEs. For the SPB, microcharcoal abundance fluctuates from

282    $2x10^4$–$4.2x10^5$ (mean $2x10^5$) particles per 10 g of sediment, and the number of macrocharcoal

283    particles varies from 99–2327 (mean 787) particles per 10 g sediment (Fig. 2, SI Table 3). A similar

284    trend is observed in both size fractions, with individual charcoal peaks fluctuating on a 2–4 m scale

285    (Fig. 2). In the higher resolution LPE interval, metre-scale individual peaks of charcoal abundance are

286    observed, with microcharcoal abundance fluctuating from $4.5x10^3$–$4.3x10^5$ (mean $1.1x10^5$) particles

287    per 10 g of sediment, and the number of macrocharcoal particles varies from 8–2276 (mean 376)

288    particles per 10 g sediment (Fig. 3, SI Table 3). Longer term fluctuations in the macrocharcoal record

289    are also observed, with bundling of peaks visible every ~4–5 m. Micro- and macro-charcoal are more

290    abundant in the SPB compared to the LPE (Fig. 4). The outcome of the Wilcoxon signed rank test

291    confirms a different median of the SPB and LPE macrocharcoal (H0 rejected, p<0.001) and

microcharcoal (H0 rejected, p<0.001).

293
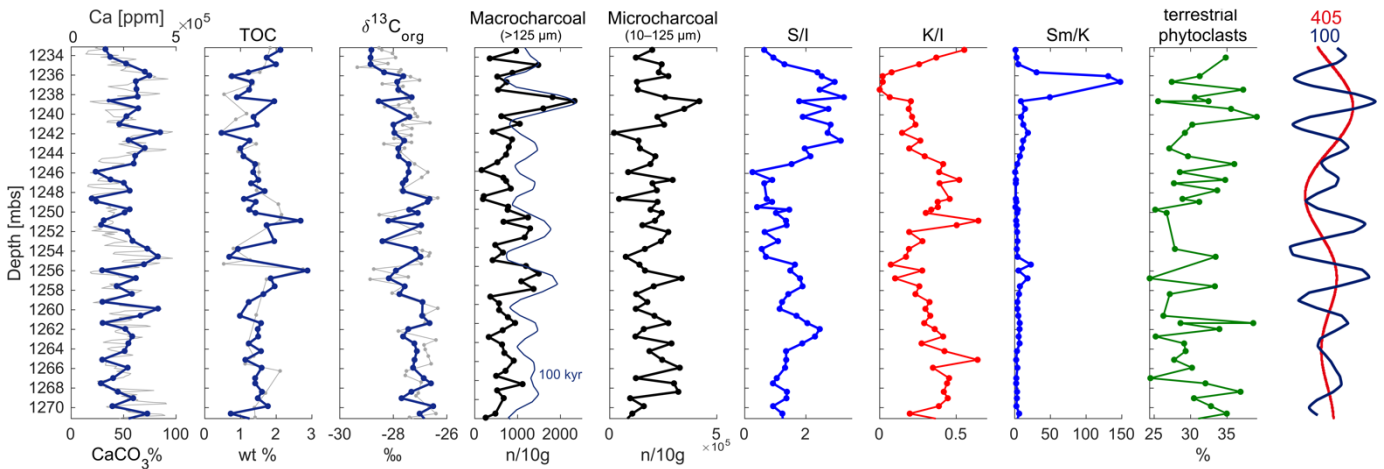


**Fig. 2:** *The SPB studied interval showing all proxies of this study in context of the orbital filters (Ruhl et al., 2016). The CaCO₃, TOC and δ¹³Cₒᵣg (blue) data obtained for the present study are plotted over previously published data (light grey – Ruhl et al., 2016; Storm et al., 2020). The macrocharcoal abundance shows ~8 increases and decreases throughout the studied interval. These high-low intervals in the macrocharcoal record correspond to the 100 kyr filter (blue; and see SI Fig. 2). The majority of macrocharcoal peaks are mirrored in the microcharcoal fraction. Alternating phases of increase in the smectite/illite ratio (S/I) and the kaolinite/illite ratio (K/I) indicate swings in the hydrological cycle. This is further indicated by the smectite/kaolinite ratio (Sm/K). The percentage of terrestrial phytoclasts shows that the terrestrially sourced organic particles fluctuate around 30% in the studied interval. Finally, the bandpass-filtered time series of the Ca-elemental XRF record of Ruhl et al. (2016) indicate that the clay records shift dominance on a 405 kyr time scale. The peaks in the macrocharcoal record occur on a 100 kyr time scale (see also SI Fig. 2).*

306
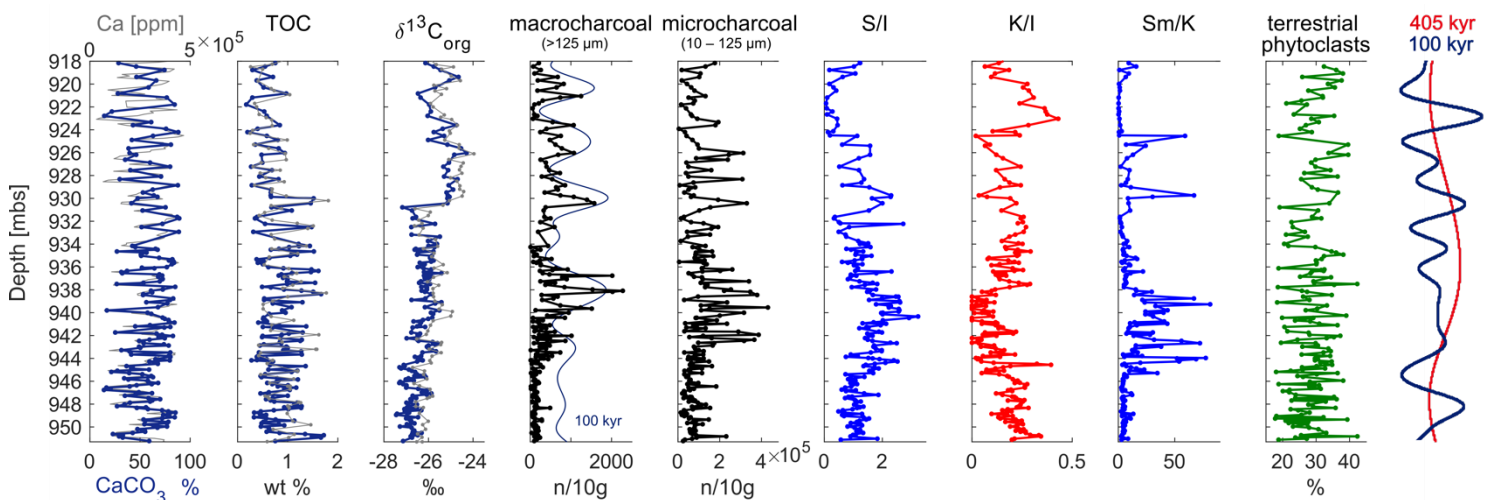


**Fig. 3: Synthesis of the LPE interval showing all proxies considered in this study in context of the**

308 ***orbital filters (Ruhl et al., 2016).*** *The CaCO$_3$, TOC and $\delta^{13}C_{org}$ (blue) from Hollaar et al. (2023) are*

309 *plotted over independently generated data (light grey - Ruhl et al., 2016; Storm et al., 2020). The*

310 *macrocharcoal abundance shows ~7 peaks throughout the studied interval. These 7 increases and*

311 *decreases in macrocharcoal abundance correspond to the 100 kyr eccentricity (in blue, see SI Fig. 2).*

312 *The majority of macrocharcoal peaks are mirrored in the microcharcoal fraction. Alternating phases*

313 *of increase in the smectite/illite ratio (S/I) and the kaolinite/illite ratio (K/I) indicate swings in the*

314 *hydrological cycle. This is further indicated by the smectite/kaolinite ratio (Sm/K). The percentage of*

315 *terrestrial phytoclasts shows that the terrestrially sourced organic particles fluctuate around 30 % in*

316 *the studied interval. Finally, the orbital filters of Ruhl et al. (2016) are placed next to the proxy*

317 *records. This shows that the clay records shift dominance on a 405 kyr time scale. The peaks in the*

318 *macrocharcoal record occur on a 100 kyr time scale.*

319

320 The palynofacies of both intervals is typically marine (AOM>58%). The proportion of terrestrial vs

321 marine organic matter remains relatively stable through both the SPB and LPE, varying between 24.4

322 and 39.1% (mean 30.7%), and 17.7 and 42.3% (mean 28.9%), respectively. Charcoal accounts for

323 ~3.7% and ~4.5% of the total particulate organic matter, respectively for the SPB and the LPE

324 intervals (SI Fig. 4). The abundance of macrocharcoal is not influenced by the percentage of terrestrial

325 particulate organic matter through the SPB and LPE intervals (SPB r = -0.12, p = 0.42; LPE r = 0.06,

326 p = 0.46) and nor is the microcharcoal abundance for the SPB interval (r = 0.07, p = 0.62). However, a

327 very weak correlation exists between the percentage of terrestrial phytoclasts and microcharcoal

328 abundance in the LPE interval (r = 0.16, p = 0.05). These results suggest that the preservation and/or

329 influx of terrestrial particulate organic matter is not the main driver of fluctuations in charcoal

330 abundance.
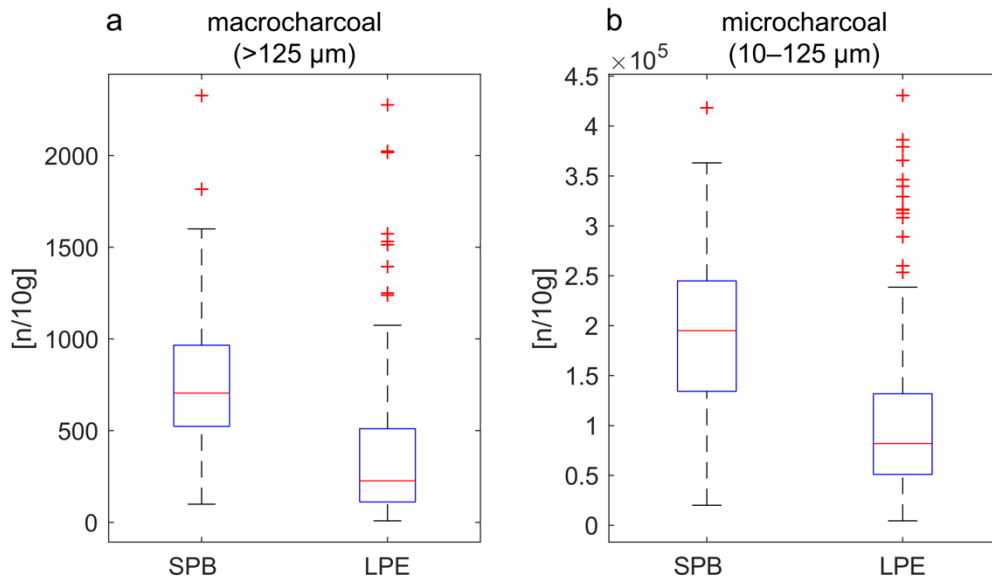
**Fig. 4:** *Distribution boxplots of the macrocharcoal and microcharcoal abundance of the SPB and LPE studied intervals. (a) Average macrocharcoal abundance is higher in the SPB interval compared to the LPE interval, however, the absolute minimum and maximum are similar. (b) Average microcharcoal abundance is higher for the SPB compared to the LPE. The minimum number of microcharcoal particles is lower for the LPE, however, the maximum microcharcoal abundance is similar in both records.*

The clay mineral assemblages of the SPB and LPE are dominated by illite, kaolinite and smectite (I-S R0), with smectite increasing in parallel with decreases of illite and kaolinite (SI Fig. 5). Low proportions of chlorite and sparse I-S R1 are present in the SPB record. Chlorite and I-S R1 are generally low in the LPE record but increase between 924–219 mbs (SI Fig. 5). Two smectite-enhanced phases occur for the SPB, at 1264–1255 mbs and 1245–1235 mbs. Both these phases are coeval with high charcoal abundance (both size fractions) (Fig. 2, SI Fig. 6). Additionally, the LPE interval encompasses two stratigraphic intervals rich in smectite; from 944–937 mbs and 931–924 mbs. Charcoal abundance (both size fractions) increases overall, and coevally with the S/I, over ~5 m scale fluctuations, and decreases at levels with high K/I (Fig. 3, SI Fig. 7). The 3.2–10.2 m orbital filter of the macrocharcoal records (interpreted as the 100 kyr eccentricity (Ruhl et al., 2016; Hinnov et al., 2018; Storm et al., 2020; Pienkowski et al., 2021)), indicates that the observed fluctuations in the macrocharcoal record occur with a 100 kyr periodicity (SI Fig. 2).

## 4 Discussion

*Charcoal transport and preservation*

The charcoal records for both the SPB and LPE intervals do not appear to be linked to the terrestrial influx of materials, as evidenced by the palynofacies. No correlation or covariance exists between the abundance of terrestrial phytoclasts and the number of charcoal particles, which suggests that the abundance of charcoal is not a reflection of preservation and/or runoff changes. Inferred sea level changes during the LPE and the SPB could potentially have impacted the charcoal abundance record and the clay mineralogy. Transgression and relative sea-level rise during the SPB has been extensively recorded from the Boreal and Tethys regions, and from South America (e.g. Legarreta and Uliana, 1996; de Graciansky et al., 1998; Hesselbo & Jenkyns, 1998; Danisch et al., 2019; Silva et al., 2021). The Late Pliensbachian is characterized by widespread regressive facies and inferred relative sea-level fall, likely indicating a closer proximity to shore also in the Mochras borehole. Fossil wood in the Mochras borehole has been shown to become more abundant at this time, suggesting a potential bias of higher terrestrial input from a nearby landmass (Ullmann et al., 2022). However, the mean abundance of macrocharcoal and microcharcoal is higher during the SPB (mean of 787 and $2x10^5$ respectively) compared to the LPE (mean of 376 and $1.1x10^5$ respectively) in the Mochras borehole, suggesting that the shore proximity did not impact overall charcoal abundance. Similarly, the palynofacies analysis indicates that the mean abundance of terrestrial particulate organic matter during the SPB (30.7%) is not higher compared to the LPE (28.9%). Hence, we take this as strong evidence that the record of fossil charcoal records changes in wildfire activity.

*Orbital forcing of the hydrological cycle and fire*

Alternations in the dominance of smectite and kaolinite occur approximately every 10 m in both the LPE and SPB records. Kaolinite and smectite reflect hydrological changes in the palaeoenvironment of the Cardigan Bay Basin (Deconinck et al., 2019; Munier et al., 2021). As the smectite and kaolinite clay minerals are detrital in character and their abundance varies in opposition to one another (Fig. 2 and 3), these clays are likely derived from pedogenic weathering profiles (Deconinck et al., 2019). Smectite preferentially forms under a warm and seasonally arid climate, similar to a monsoonal climate system or the winter-wet climate of the Mediterranean zone (Chamley, 1989; Deconinck et al., 2019). Kaolinite is indicative of an accelerated hydrological cycle and an intensification of hydrolysis, increased runoff and a year-round wet climate (Chamley, 1989; Ruffell et al., 2002) either via formation in strong weathering profiles or via the physical erosion of kaolinite-bearing rocks (Chamley, 1989). Pedogenic kaolinite preferentially forms in a hot climate (Chamley, 1989; Ruffell et al., 2002). At times of high smectite abundance, fire activity is greatest as observed from the macro- and micro-scopic charcoal fractions (Fig. 2 and 3). Based on the astrochronological framework of the Mochras borehole (Ruhl et al., 2016; Hinnov et al., 2018; Storm et al., 2020; Pieńkowski et al., 2021) these alternations appear to occur in concert with the 405 kyr long-eccentricity cycles (Fig. 2, Fig. 3). Eccentricity modulates the precession driven changes in seasonal and latitudinal distribution of insolation (Imbrie & Imbrie, 1980; Berger et al., 1989). One ~20 kyr precession cycle can represent a

strongly seasonal extreme climate for ~10 kyr and a weakly seasonal climate for the subsequent ~10 kyr. The geological record averages the amplification or suppression of seasonality between years (SI Fig. 8). Eccentricity forcing modulates the amplitudes of these extremes in seasonality with periodicities of 100 kyr and 405 kyr.

In the Mesozoic, eccentricity maxima are commonly associated with dry climates that are disrupted by short and intense periods of precipitation and storm activity in the boreal landmasses bordering the NW Tethys (Martinez & Dera, 2015). In contrast, eccentricity minima are characterized by a more moderate seasonal contrasts and year-round wet conditions (Martinez & Dera, 2015). Eccentricity minima are linked to periods of enhanced runoff and weathering conditions as evidenced by high kaolinite content, $^{87}Sr/^{86}Sr$, and negative shifts in $\delta^{18}O$ (Martinez & Dera, 2015). Therefore, we link the observed smectite-rich intervals to eccentricity maxima and the kaolinite-rich intervals to eccentricity minima. Charcoal abundance is highest during the seasonal climate of the eccentricity maxima for the SPB (Fig. 2 and 3), in agreement with the previous findings for the LPE (Hollaar et al., 2021, 2023).

Both the LPE and SPB study intervals span two 405-kyr cycles (Ruhl et al., 2016; Hinnov et al., 2018; Storm et al., 2020; Pieńkowksi et al., 2021). The relative abundance of smectite and the abundance of charcoal both reach a peak during the maxima in the long eccentricity cycle, supporting the notion that orbitally driven changes in seasonal contrast in hydrolysis led to high fire activity. Within these long-term trends, the macrocharcoal record also shows ~5 m scale individual peaks or clusters in both the LPE and SPB records (SI Fig. 2, Fig. 2 and 3). Based on the existing age model (Ruhl et al., 2016; Hinnov et al., 2018; Storm et al., 2020; Pieńkowksi et al., 2021) we derive that this is the expression of the ~100 kyr eccentricity cycle in the macrocharcoal record. The bandpass-filtered time series representing the ~100 kyr cycle in the Pliensbachian of the Mochras core (derived from the Ca and macrocharcoal records), captures the observed ~5 m oscillations in the fire record (SI Fig. 2, Fig. 2 and 3) (Ruhl et al., 2016; Hinnov et al., 2018; Storm et al., 2020; Pieńkowski et al., 2021).

The Sinemurian–Pliensbachian transition is generally associated with an overall warm and humid climate (Korte & Hesselbo, 2011; Gómez et al., 2016), and enhanced levels of runoff and weathering (Bougeault et al., 2017). The results presented here suggest that within this overall warm and humid background, orbital forcing created year-round wet periods, that were not conducive to frequent fire, alternating with periods that remained warm but had a more seasonal climate, that allowed ignition during the dry season. In contrast, the LPE, and the sediments of late Margaritatus ammonite chronozone formed in an overall semi-arid climate with proposed lower runoff levels from the land into the sea (Deconinck et al., 2019; Hollaar et al., 2021; 2023). During the run-up of the LPE we infer orbitally forced alternating climatic states of more extreme seasonality (high fire and smectite) and a more equitable year-round wet climate (low fire and high kaolinite) (Hollaar et al., 2021; 2023)

acting within this overall semi-arid climate phase. Overall, kaolinite fluctuates in abundance in opposition to smectite, reflecting hydrological changes from wet and hot to semi-arid and hot, in agreement with high fire activity during a seasonal climate and fire suppression during a year-round wet climate for both the LPE and the SPB.

*Vegetation, fire and the intermediate fire-productivity gradient*

Fuel (vegetation biomass) and moisture status of the fuel, as governed by seasonal patterns in precipitation and temperature, are the core factors that influence fire behaviour and fire regime (Archibald et al., 2009; Cochrane & Ryan, 2009; Bradstock, 2010; Archibald et al., 2013; Bowman et al., 2014; Archibald et al., 2018). Ecosystems with limited wildfire activity are generally associated with either high precipitation and abundant primary productivity, or low productivity under strongly arid conditions (Pausas & Paula, 2012). In contrast, high wildfire activity occurs in climates that are in the middle of the productivity gradient, where during moist periods plant growth is rapid and biomass builds up forming a connected fuel structure. When followed by periods of drought the fuel moisture content is lowered enabling fire ignition and spread (Pausas & Paula, 2012). Additionally, higher sensitivity to fuel moisture levels in the tropical or mesic areas have been noted, where a small fall in fuel moisture content can lead to more flammable conditions (Cochrane, 2003). Such that the mid points in the intermediate fire-productivity gradient are further enhanced. The intermediate fire-productivity hypothesis (Pausas & Bradstock, 2007; Pausas & Ribeiro, 2013) conceptualizes this relationship between climate-vegetation-fire, where fire activity is plotted along an aridity and productivity gradient (Fig. 5). The observed alternating modes of high and low fire activity, as inferred from the lower Jurassic fossil charcoal record, during the onset of the SPB and LPE, likely indicates shifts in seasonality of the Cardigan Bay Basin hinterland and would place both the LPE and the SPB at intermediate productivity levels during maximum eccentricity forcing. The deep time combined fire and hydrological records we present here are in agreement with the intermediate productivity hypothesis of Pausas & Bradstock (2007) and indicate that even the very different plant functional types and different vegetation assemblages, e.g., a world without grasses, were still subject to this overall fire-productivity gradient control. We indicate on Fig. 5 how these ecosystems without grasses and other flowering plants may have looked in respect to typical Jurassic fuel compositions. We suggest that both the LPE and the SPB switched between a state of low fire (either limited by climatic aridity or the presence and presence and connectivity of fuel) and a state of high fire during which seasonal contrast is high and an ideal 'fire window' exists in which biomass built up during the wet season after which a fire-prone season followed (Fig. 5).
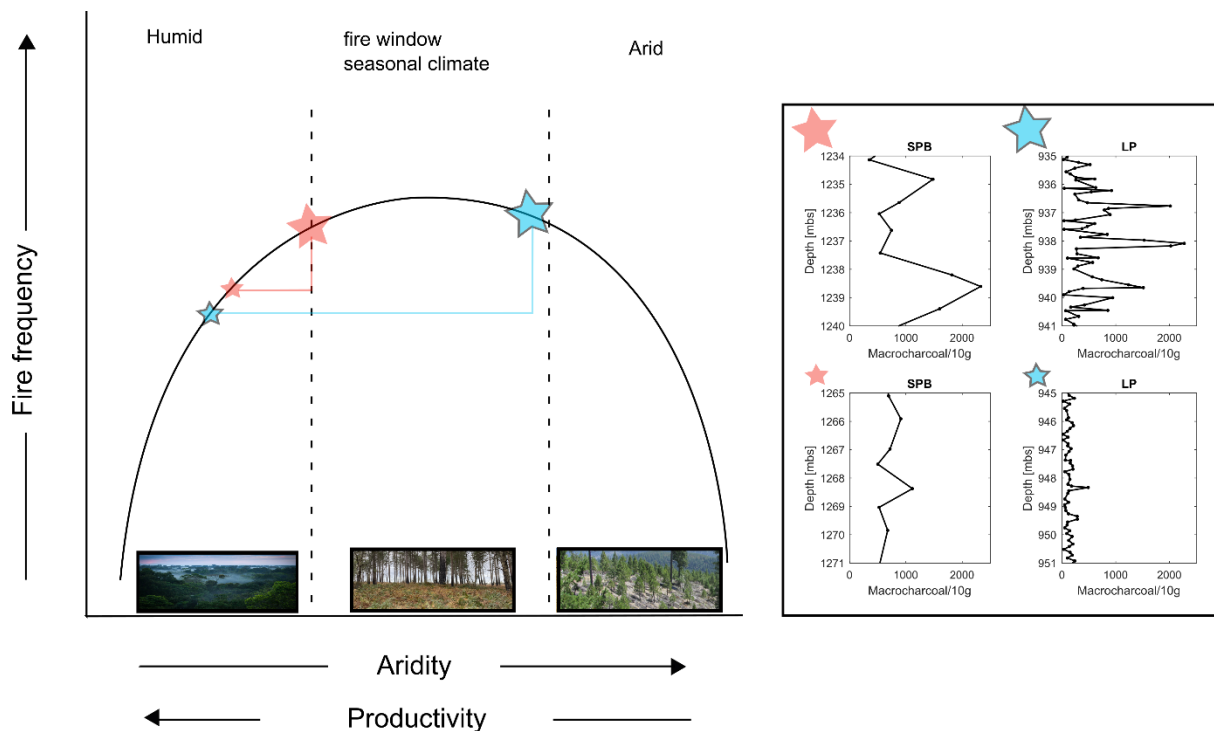
**Fig. 5: The LPE and SPB fire records placed on the intermediate productivity gradient.** *The graph is adapted from Pausas & Bradstock (2007). Fire frequency is highest in the middle of the hyperbola, medium levels of aridity and productivity created a seasonal climate in which seasonal biomass growth was possible (productivity) and seasonally the fuel moisture limits were lower in a season of drought (aridity), this created the optimized 'fire window'. The SPB is plotted on this fire-productivity gradient in red: the small star indicates the eccentricity minimum state and the large star the eccentricity maximum state. The LPE is plotted on the fire-productivity gradient in blue, and again the small star indicates the eccentricity minimum and the large star the eccentricity maximum. The LPE has a larger range compared to the SPB, and experienced more fire suppression due to high humidity levels during eccentricity minima, and also was closer to a productivity limitation state during the eccentricity maximum.*

The studied Early Jurassic time-interval likely had five distinct biomes; a seasonal dry (summerwet or subtropical) biome in the low latitudes, a desert biome in the subtropics, narrow latitudinal bands of a winterwet biome at low-mid latitude, and warm temperate and cool temperate biomes at mid- and high-latitudes, respectively (Rees et al., 2000; Willes and McElwain, 2014). The Cardigan Bay Basin was likely positioned within the winterwet biome at approximately 35 °N (Torsvik et al., 2017). It therefore would have sat within the bounds of the fire window of the intermediate fire-productivity hypothesis (Fig. 5). The winterwet biome in both the Sinemurian and Pliensbachian stages were dominated by conifers as the canopy tree, with a mid-canopy vegetation of cycads and tree-ferns, and an understory mixture of seed ferns, horsetails and ferns that likely flourished during wetter periods (Rees et al., 2000; Slater et al., 2019; Bos et al., 2023). This is evidenced from sporomorph data from the Mochras borehole that hosts abundant fossil pollen in the Sinemurian and Pliensbachian (>94%)

17

(Van de Schootbrugge et al., 2005). Additionally, nearby locations also show evidence of orbitally paced shifts in vegetation assemblages from sites at St. Audries Bay, UK and in NW Germany (Bonis et al., 2010; Bos et al., 2023).

During the 100 kyr eccentricity maxima in the UK pollen from the dry-adapted cheirolepidacean conifers is found to be highly abundant (Bonis et al., 2010). Whilst, in Germany a mire-conifer community is apparent with sporomorphs indicating variations in abundance of ferns and fern allies occurring over a 405-kyr eccentricity cycle, with ferns most abundant during eccentricity maxima (Bos et al., 2023).

Dry-adapted vegetation, such as the cheirolepidacean conifers likely thrived during more extreme seasonal droughts, maintaining their biomass. In contrast, ferns and fern allies, and mire-conifers as humid-loving plants would grow rapidly during sustained, year-round, periods of rainfall (eccentricity minima), likely inhabiting both open environments and colonising the understory of conifer forests. Furthermore, these humid-loving plants would also be able to build dense connected fuel loads during the wet-season of eccentricity maxima, that were then readily dried during the annual dry-season. Ferns, when cured, carry high intensity fires (Adie et al., 2011; Belcher and Hudspith, 2016) and during the Mesozoic 'fern prairies' have been linked to intense surface fires (Harris, 1981; Van Konijnenburg-Van Cittert, 2002; Collinson et al., 2007, 2009). Hence, they are suggested to have functioned in a similar fashion to support fires as grasslands and fern stands do today; Mesozoic fern prairies and savannahs therefore likely filled a similar ecological niche to grasses in the modern day (Belcher, 2013 and references therein). Ferns are indeed a common feature of Mesozoic charcoal assemblages, showing their association with fire throughout time (e.g. Collinson et al., 2000; Brown et al., 2012).

In the present-day, temperature is an important regulator of fire occurrence. Whilst dead fuel moisture (e.g. that of litter and cured herbaceous components) is primarily influenced by the variability in relative humidity, live fuels are controlled by the combination of temperature and moisture availability, where long periods of drought or heat wave extremes can strongly influence the flammability of live fuels. Sea surface temperatures during the Sinemurian and Pliensbachian were at times apparently higher than 28 °C (Robinson et al., 2017). But high-resolution temperature reconstructions are lacking for the Early Jurassic. Orbital forcing of regional–global seawater temperatures occurred throughout the Cenozoic (Westerhold et al., 2020), and likely also the Mesozoic; however, the climate response to changes in orbital insolation is non-linear, and the mean annual insolation is not impacted by precession (Rubicam, 1994). Therefore, the biomes of the SPB not only existed in an overall warm world that was characterized by background orbitally driven climate shifts across the moister side of the fire-productivity gradient, but superimposed on this live fuels were also responsive to extreme weather linked to periods of drought and heat.

516

517  We propose that the overall humid climate of the SPB fits the high productivity scenario, in which the

518  frequency of flammable conditions is the main factor controlling fire occurrences. No evidence was

519  found to place the SPB on the productivity-limiting high-aridity side of the fire-productivity gradient,

520  where fire frequency would have been mainly influenced by enhanced rainfall in an otherwise dry

521  climate. These findings are in line with the presence of plant cuticle through the studied record,

522  indicating the presence of vegetation throughout this time period and during both phases of high and

523  low modes of fire activity. Hence, the SPB seems to conform to the humid and high productivity end

524  of the aridity gradient (Fig. 5 red lines). Within these constraints (Fig. 5) the SPB is characterized by

525  likely two states across the fire productivity gradient. The biome was situated at the wetter, low fire

526  side of the fire-productivity gradient during eccentricity minima (Fig. 5), and at the seasonal, high fire

527  end of the fire-productivity gradient during eccentricity maxima (but only for each precession half-

528  cycle) (Fig. 5).

529  The fluctuations detected in the present study for the SPB occurred over both long-eccentricity and

530  short eccentricity timescales in the macrocharcoal record, showing longer phases of overall

531  enhancement of fire (405 kyr eccentricity) and relatively abrupt shifts from low to high fire and back

532  again (~100 kyr eccentricity). For this reason, the SPB is placed on a steep portion of the fire-

533  productivity gradient curve (Fig. 5). Overall, the mean charcoal abundance is relatively high, and no

534  sustained periods of very low charcoal abundance are observed in the SPB record, which indicates

535  that the climate never became too wet to fully limit fire activity at that time.

536  The Late Pliensbachian has been linked to a global cooling event, with a potential of 5–7 °C lowering

537  in temperature inferred for the NW Tethys region (Korte et al., 2015). The atmospheric moisture

538  holding capacity of a cooler climate is lower compared to a warm climate, in which a 1 °C cooling

539  likely lowers the water holding capacity of air by 7% (Trenberth et al., 2005). The presence of

540  terrestrial phytoclasts throughout confirms the presence of vegetation in the surrounding landmasses

541  throughout this period. The mean abundance of charcoal for the LPE section is slightly lower than that

542  of the SPB and the lowest charcoal abundances are coeval with a K/I enhancement, suggesting that

543  during eccentricity minima environmental conditions moved further into the humid zone of the fire-

544  productivity gradient (Fig. 5 blue line). Increasing eccentricity shifted the system to a more seasonal

545  climate where the fire and clay records indicate the presence of a wet season that allowed for build-up

546  of biomass followed by a dry season in which fire was able to be ignited and spread.

547  Conceptually, the relatively drier and cooler LPE climate would have resulted in conditions that are

548  more arid, shifting to the biomass-limited part of the productivity/aridity – fire frequency gradient

549  during eccentricity maxima, compared to the SPB (Fig. 5 blue lines). This is supported by the large

550  fluctuations observed between low fire frequency and high fire frequency for the LPE and the fact that

estimated high fire periods did not occur suddenly, but rather were sustained over a larger part of the cycle. Therefore, the phase of highest fire frequency operating in the seasonal 'fire window' as indicated in figure 5 for the LPE (blue lines) likely occurred for a larger part of the fire productivity gradient. Hence, conditions across the LPE occurred across a wider range of the productivity/aridity and fire frequency gradients (Fig. 5 blue lines) compared to the SPB. There is no evidence that conditions ever became limited by aridity, and conditions during the LPE did not extend beyond the seasonal fire window into the arid part of the productivity/aridity gradient.

Importantly, the Jurassic climate was overall warm and humid, about 5–10 °C warmer on global average compared to today (e.g., Rees et al., 2000; Sellwood & Valdes, 2008), with ~3.5–10 times the pre-industrial value of atmospheric $p$CO$_2$ during the Early Jurassic (e.g. Retallack, 2001; Beerling & Royer, 2002; McElwain et al., 2005; Berner, 2006; Steinthorsdottir & Vajda, 2015; Li et al., 2020). In this context, it may not be surprising that a relative cooling event in the Early Jurassic did not lead to the aridity and biomass-limiting conditions observed during the last glacial period, at latitudes of ~38 °C N (Daniau et al., 2007).

**5 Conclusions**

The study of two different climatic 'background' states, at the LPE and the SPB, shows that fire activity was strongly modulated by orbital eccentricity cycles. The 405 kyr shifts in the record of wildfire prevalence reflect similar changes also in the hydrological cycle (based on clay mineralogy data) showing that high fire activity occurred during periods of high seasonal contrast and that fire activity was suppressed during periods of high year-round humidity, because the latter would have enhanced the fuel moisture levels and prevented frequent ignition and sustained fire spread. The fire record of both climatic events is limited by the high fuel moisture levels during eccentricity minima, but fires were more prevalent during times of increased seasonality, every precession half-cycle during eccentricity maxima. Hence, during both events fire activity was limited by fuel moisture content and not by productivity. Both the SPB and the LPE climate systems were therefore situated on the moisture-limited side of the intermediate fire-productivity gradient (Fig. 5). Due to the lower moisture-holding capacity of cold air, the overall higher seasonality of the Late Pliensbachian and the more sustained high fire-frequency periods (based on the charcoal record for the LPE) we place the LPE towards the higher end of the aridity gradient, within maximum seasonality and maximum fire frequency window of the fire productivity graph (Fig. 5). The SPB fire regime reflected a more humid climate that shifted abruptly between low fire frequency to high fire frequency within less extreme bounds on the aridity gradient. This research reveals that the intermediate-fire productivity hypothesis (Pausas & Bradstock, 2007) can also be applied to high-resolution deep time records, before the evolution of grasses and that this hypothesis explains well the influence of orbital cycles within different overall climate states, be they cooling or warming trends. The coupling of high-resolution clay mineralogy and fossil charcoal records, combined with constraints on orbital forcing at such

587 time, allows for inferences on how Earth's natural climate state variability has driven shifts in
588 terrestrial productivity through the geological past.

**Conflict of Interest**

599 The authors declare no conflicts of interest relevant to this study.

**Data Availability Statement**

601 Supplementary data are available at the National Geoscience Data Centre at Keyworth (NGDC)
602 at https://doi.org/10.5285/1461dbe5-50a8-425c-8c49-ac1f04bcc271 (Hollaar, 2022) for the interval
603 934–918 m. b.s. All data presented for the interval 951–934 m. b.s. are available at the National
604 Geoscience Data Centre at Keyworth (NGDC) at https://doi.org/10.5285/d6b7c567-49f0-44c7-a94c-
605 e82fa17ff98e (Hollaar et al., 2021b). All data for the interval 1271–1233 mbs are available at the
606 National Geoscience Data Centre at Keyworth (NGDC) at https://doi.org/10.5285/2ec864e0-cb08-
607 44c0-92fe-07af2ef93e3a

**Supporting Information**

609

**References**

611 Adie, H., Richert, S., Kirkman, K. P., & Lawes, M. J. (2011). The heat is on: frequent high intensity
612 fire in bracken (Pteridium aquilinum) drives mortality of the sprouting tree Protea caffra in temperate
613 grasslands. *Plant Ecology*, 212, 2013 – 2022. https://doi.org/10.1007/s11258-011-9945-8

614 Archibald, S., Lehmann, C. E., Belcher, C. M., Bond, W. J., Bradstock, R. A., Daniau, A. L., et al.
615 (2018). Biological and geophysical feedbacks with fire in the Earth system. *Environmental Research*
616 *Letters*, 13(3), 033003. https://doi.org/10.1088/1748-9326/aa9ead

617 Archibald, S., Lehmann, C. E., Gómez-Dans, J. L., & Bradstock, R. A. (2013). Defining pyromes and
618 global syndromes of fire regimes. *Proceedings of the National Academy of Sciences*, 110(16), 6442 –
619 6447. https://doi.org/10.1073/pnas.1211466110

620 Archibald, S., Roy, D. P., van Wilgen, B. W., & Scholes, R. J. (2009). What limits fire? An
621 examination of drivers of burnt area in Southern Africa. *Global Change Biology*, 15(3), 613 – 630.
622 https://doi.org/10.1111/j.1365-2486.2008.01754.x

623 Beerling, D. J., & Royer, D. L. (2002). Fossil plants as indicators of the Phanerozoic global carbon
624 cycle. *Annual Review of Earth and Planetary Sciences*, 30(1), 527 – 556.
625 https://doi.org/10.1146/annurev.earth.30.091201.141413

626 Belcher, C. M., Collinson, M. E., & Scott, A. C. (2005). Constraints on the thermal energy released
627 from the Chicxulub impactor: new evidence from multi-method charcoal analysis. *Journal of the*
628 *Geological Society*, 162(4), 591 – 602. https://doi.org/10.1144/0016-764904-104

629 Belcher, C. M., Collinson, M. E., & Scott, A. C. (2013). A 450-Million-Year History of Fire. In C. M.
630 Belcher (Eds.). Fire Phenomena and the Earth System. (pp. 240 – 241). London, UK: Wiley.

631 Belcher, C. M., & Hudspith, V. A. (2017). Changes to Cretaceous surface fire behaviour influenced
632 the spread of the early angiosperms. *New Phytologist*, 213(3), 1521 – 1532.
633 https://doi.org/10.1111/nph.14264

634 Berger, A., Loutre, M. F. & Dehant, V. Astronomical frequencies for pre-Quaternary palaeoclimate
635 studies. *Terra Nova 1*, 474–479 (1989). https://doi.org/10.1111/j.1365-3121.1989.tb00413.x

636 Berner, R. A. (2006). GEOCARBSULF: a combined model for Phanerozoic atmospheric O2 and
637 CO2. *Geochimica et Cosmochimica Acta*, 70(23), 5653 – 5664.
638 https://doi.org/10.1016/j.gca.2005.11.032

639 Bonis, N. R., Ruhl, M., & Kürschner, W. M. (2010). Milankovitch-scale palynological turnover across
640 the Triassic–Jurassic transition at St. Audrie's Bay, SW UK. *Journal of the Geological Society*, 167(5),
641 877 – 888. https://doi.org/10.1144/0016-76492009-141

642 Bos, R., Lindström, S., van Konijnenburg-van Cittert, H., Hilgen, F., Hollaar, T. P., Aalpoel, H. et al.
643 (2023). Triassic-Jurassic vegetation response to carbon cycle perturbations and climate
644 change. *Global and Planetary Change*, 228, 104211. https://doi.org/10.1016/j.gloplacha.2023.104211

645 Bougeault, C., Pellenard, P., Deconinck, J. F., Hesselbo, S. P., Dommergues, J. L., Bruneau, L., et al.
646 (2017). Climatic and palaeoceanographic changes during the Pliensbachian (Early Jurassic) inferred
647 from clay mineralogy and stable isotope (CO) geochemistry (NW Europe). *Global and Planetary*
648 *Change*, 149, 139 – 152. https://doi.org/10.1016/j.gloplacha.2017.01.005

649 Bowman, D. M., Murphy, B. P., Williamson, G. J., & Cochrane, M. A. (2014). Pyrogeographic
650 models, feedbacks and the future of global fire regimes. *Global Ecology and Biogeography*, 23(7),
651 821 – 824. https://doi.org/10.1111/geb.12180

652    Bradstock, R. A. (2010). A biogeographic model of fire regimes in Australia: current and future

653    implications. *Global Ecology and Biogeography*, 19(2), 145 – 158. https://doi.org/10.1111/j.1466-

654    8238.2009.00512.x

655    Brown, S. A., Scott, A. C., Glasspool, I. J., & Collinson, M. E. (2012). Cretaceous wildfires and their

656    impact on the Earth system. *Cretaceous research*, 36, 162 – 190.

657    https://doi.org/10.1016/j.cretres.2012.02.008

658    Chamley, H. (1989). Clay Sedimentology. Heidelberg: Springer Berlin Heidelberg.

659    Cochrane, M. A. (2003). Fire science for rainforests. *Nature*, 421(6926), 913 – 919.

660    https://doi.org/10.1038/nature01437

661    Cochrane, M. A., & Ryan, K. C. (2009). Fire and fire ecology: Concepts and principles. *Tropical fire*

662    *ecology*, 25 – 62. https://doi.org/10.1007/978-3-540-77381-8_2

663    Collinson, M.E, Featherstone, C. Cripps, J.A, Nichols, G.J. & Scott, A.C. (2000). Charcoal-rich plant

664    debris accumulations in the Lower Cretaceous of the Isle of Wight, England. *Acta Palaeobotanica*,

665    Supplement 2, 93 – 105.

666    Collinson, M. E., Steart, D. C., Harrington, G. J., Hooker, J. J., Scob, A. C., Allen, L. O. et al. (2009).

667    Palynological evidence of vegetation dynamics in response to palaeoenvironmental change across the

668    onset of the Paleocene-Eocene Thermal Maximum at Cobham, Southern England. *Grana*, 48(1), 38 –

669    66. https://doi.org/10.1080/00173130802707980

670    Collinson, M. E., Steart, D. C., Scob, A. C., Glasspool, I. J., & Hooker, J. J. (2007). Episodic fire,

671    runoff and deposition at the Palaeocene–Eocene boundary. *Journal of the Geological Society*, 164(1),

672    87 – 97. https://doi.org/10.1144/0016-76492005-185

673    Daniau, A. L., Bartlein, P. J., Harrison, S. P., Prentice, I. C., Brewer, S., Friedlingstein, P., et al.

674    (2012). Predictability of biomass burning in response to climate changes. Global Biogeochemical

675    Cycles, 26(4). https://doi.org/10.1029/2011GB004249

676    Daniau, A. L., Sánchez-Goñi, M. F., Beaufort, L., Laggoun-Défarge, F., Loutre, M. F., & Duprat, J.

677    (2007). Dansgaard–Oeschger climatic variability revealed by fire emissions in southwestern

678    Iberia. *Quaternary Science Reviews*, *26*(9-10), 1369 – 1383.

679    https://doi.org/10.1016/j.quascirev.2007.02.005

680    Danisch, J., Kabiri, L., Nutz, A., & Bodin, S. (2019). Chemostratigraphy of late Sinemurian–early

681    Pliensbachian shallow-to deep-water deposits of the Central High Atlas Basin: Paleoenvironmental

682 implications. *Journal of African Earth Sciences*, 153, 239 – 249.

683 https://doi.org/10.1016/j.jafrearsci.2019.03.003

684 Deconinck, J. F., Hesselbo, S. P., & Pellenard, P. (2019). Climatic and sea-level control of Jurassic

685 (Pliensbachian) clay mineral sedimentation in the Cardigan Bay Basin, Llanbedr (Mochras Farm)

686 borehole, Wales. *Sedimentology*, 66(7), 2769 – 2783. https://doi.org/10.1111/sed.12610

687 De Graciansky, P. C., Dardeau, G., Dommergues, J. L., Durlet, C., Marchand, D., Dumont, T., et al.

688 (1998). Ammonite biostratigraphic correlation and Early Jurassic sequence stratigraphy in France:

689 comparisons with some UK sections. In: de Graciansky, P.C., Hardenbol, J., Jacquin, T., Farley, M. &

690 Vail, P.R. (Eds.), Mesozoic and Cenozoic Sequence Statigraphy of European Basins. *Special*

691 *Publication of the Society for Sedimentary Geology (SEPM)*, 60, 583 – 622.

692 Glasspool, I. J., Edwards, D., & Axe, L. (2004). Charcoal in the Silurian as evidence for the earliest

693 wildfire. *Geology*, *32*(5), 381 – 383. https://doi.org/10.1130/G20363.1

694 Glasspool, I. J., & Gastaldo, R. A. (2022). Silurian wildfire proxies and atmospheric oxygen.

695 *Geology*. https://doi.org/10.1130/G50193.1

696 Gómez, J. J., Comas-Rengifo, M. J., & Goy, A. (2016). Palaeoclimatic oscillations in the

697 Pliensbachian (Early Jurassic) of the Asturian Basin (Northern Spain). *Climate of the Past*, 12(5),

698 1199 – 1214. https://doi.org/10.5194/cp-12-1199-2016

699 Hammer, Ø., Harper, D. A. T., Ryan, P. D. 2001. PAST: Paleontological statistics software package

700 for education and data analysis. *Palaeontologia Electronica*, 4(1): 9pp. http://palaeo-

701 electronica.org/2001_1/past/issue1_01.htm

702 Harris, T. M. (1981). Burnt ferns from the English Wealden. *Proceedings of the Geologists'*

703 *Association*, 92(1), 47 – 58. https://doi.org/10.1016/S0016-7878(81)80019-3

704 Haq, B. U. (2018). Jurassic sea-level variations: a reappraisal. *GSA today*, 28(1), 4 – 10.

705 https://doi.org/10.1130/GSATG359A.1

706 Hinnov, L. A., Ruhl, M. R., & Hesselbo, S. P. (2018). Reply to the Comment on "Astronomical

707 constraints on the duration of the Early Jurassic Pliensbachian Stage and global climatic fluctuations"

708 (Ruhl *et al*., (2016). *Earth and Planetary Science Letters*, 455, 149 – 165).

709 https://doi.org/10.1016/j.epsl.2017.10.061

710 Hesselbo, S.P. & Jenkyns, H.C. (1998). British Lower Jurassic sequence stratigraphy. In: de

711 Graciansky, P.C., Hardenbol, J., Jacquin, T., Farley, M. & Vail, P.R. (Eds.), Mesozoic–Cenozoic

712 Sequence Stratigraphy of European Basins. *Special Publication of the Society for Sedimentary*

713 *Geology (SEPM)*, 60, 561 – 581.

714 Hollaar, T. P., Baker, S. J., Hesselbo, S. P., Deconinck, J. F., Mander, L., Ruhl, M., & Belcher, C. M.
715 (2021). Wildfire activity enhanced during phases of maximum orbital eccentricity and precessional
716 forcing in the Early Jurassic. *Communications Earth & Environment*, 2(1), 1 – 12.
717 https://doi.org/10.1038/s43247-021-00307-3

718 Hollaar, T. P., Hesselbo, S. P., Deconinck, J. F., Damaschke, M., Ullmann, C. V., Jiang, M., &
719 Belcher, C. M. (2023). Environmental changes during the onset of the Late Pliensbachian Event
720 (Early Jurassic) in the Cardigan Bay Basin, Wales. Climate of the Past, 19(5), 979-997.
721 https://doi.org/10.5194/cp-19-979-2023

722 Imbrie, J., & Imbrie, J. Z. (1980). Modeling the climatic response to orbital variations. *Science*,
723 207(4434), 943 – 953. https://doi.org/10.1126/science.207.4434.943

724 Korte, C. & Hesselbo, S. P. (2011). Shallow marine carbon and oxygen isotope and elemental records
725 indicate icehouse-greenhouse cycles during the Early Jurassic. *Paleoceanography*, 26(4).
726 https://doi.org/10.1029/2011PA002160

727 Korte, C., Hesselbo, S. P., Ullmann, C. V., Dietl, G., Ruhl, M., Schweigert, G., & Thibault, N. (2015).
728 Jurassic climate mode governed by ocean gateway. *Nature communications*, 6(1), 1 – 7.
729 https://doi.org/10.1038/ncomms10015

730 Krawchuk, M. A., & Moritz, M. A. (2011). Constraints on global fire activity vary across a resource
731 gradient. *Ecology*, 92(1), 121 – 132. https://doi.org/10.1890/09-1843.1

732 Legarreta, L., & Uliana, M. A. (1996). The Jurassic succession in west-central Argentina: stratal
733 patterns, sequences and paleogeographic evolution. *Palaeogeography, Palaeoclimatology,*
734 *Palaeoecology*, 120(3-4), 303 – 330. https://doi.org/10.1016/0031-0182(95)00042-9

735 Li, X., Wang, J., Rasbury, T., Zhou, M., Wei, Z., & Zhang, C. (2020). Early Jurassic climate and
736 atmospheric CO 2 concentration in the Sichuan paleobasin, southwestern China. *Climate of the Past*,
737 16(6), 2055 – 2074. https://doi.org/10.5194/cp-16-2055-2020

738 Martinez, M. & Dera, G. (2015). Orbital pacing of carbon fluxes by a ∼ 9-My eccentricity cycle
739 during the Mesozoic. *Proceedings of the National Academy of Sciences*, 112, 12604 – 12609.
740 https://doi.org/10.1073/pnas.141994611

741 McElwain, J. C., Wade-Murphy, J., & Hesselbo, S. P. (2005). Changes in carbon dioxide during an
742 oceanic anoxic event linked to intrusion into Gondwana coals. *Nature*, 435(7041), 479 – 482.
743 https://doi.org/10.1038/nature03618

744    Meyn, A., White, P. S., Buhk, C., & Jentsch, A. (2007). Environmental drivers of large, infrequent

745    wildfires: the emerging conceptual model. *Progress in Physical Geography*, 31(3), 287 – 312.

746    https://doi.org/10.1177/0309133307079365

747    Moore, D. M. & Reynolds Jr, R. C. (1997). *X-ray Diffraction and the Identification and Analysis of*

748    *Clay Minerals*. Oxford: Oxford University Press.

749    Munier, T., Deconinck, J. F., Pellenard, P., Hesselbo, S. P., Riding, J. B., Ullmann, C. V., et al.

750    (2021). Million-year-scale alternation of warm–humid and semi-arid periods as a mid-latitude climate

751    mode in the Early Jurassic (late Sinemurian, Laurasian Seaway). *Climate of the Past*, 17(4), 1547 –

752    1566. https://doi.org/10.5194/cp-17-1547-2021

753    Oboh-Ikuenobe, F. E., Obi, C. G. & Jaramillo, C. A. (2005). Lithofacies, palynofacies, and sequence

754    stratigraphy of Palaeogene strata in Southeastern Nigeria. *Journal of African Earth Sciences*, 41, 79–

755    101. https://doi.org/10.1016/j.jafrearsci.2005.02.002

756    Pausas, J. G., & Bradstock, R. A. (2007). Fire persistence traits of plants along a productivity and

757    disturbance gradient in mediterranean shrublands of south-east Australia. *Global Ecology and*

758    *Biogeography*, 16(3), 330 – 340. https://doi.org/10.1111/j.1466-8238.2006.00283.x

759    Pausas, J. G., & Paula, S. (2012). Fuel shapes the fire–climate relationship: evidence from

760    Mediterranean ecosystems. *Global Ecology and Biogeography*, 21(11), 1074 – 1082.

761    https://doi.org/10.1111/j.1466-8238.2012.00769.x

762    Pausas, J. G., & Ribeiro, E. (2013). The global fire–productivity relationship. *Global Ecology and*

763    *Biogeography*, 22(6), 728 – 736. https://doi.org/10.1111/geb.12043

764    Petschick, R. MacDiff 4.1. 2. Powder diffraction software (2000). Available from the author at

765    http://www.geol.uni-erlangen.de/html/software/Macdiff.html.

766    Pieńkowski, G., Uchman, A., Ninard, K., & Hesselbo, S. P. (2021). Ichnology, sedimentology, and

767    orbital cycles in the hemipelagic Early Jurassic Laurasian Seaway (Pliensbachian, Cardigan Bay

768    Basin, UK). *Global and Planetary Change*, 207, 103648.

769    https://doi.org/10.1016/j.gloplacha.2021.103648

770    Rees, P. M., Ziegler, A. M. & Valdes, P. J. (2000). Jurassic phytogeography and climates: new data

771    and model comparisons. In Huber, B. T., Macleod, K. G. & Wing, S. L. (Eds.), *Warm Climates in*

772    *Earth History*. (pp. 297 – 318). Cambridge: Cambridge University Press.

773    Retallack, G. J. (2001). A 300-million-year record of atmospheric carbon dioxide from fossil plant

774    cuticles. *Nature*, 411(6835), 287 – 290. https://doi.org/10.1038/35077041

775   Riding, J. B., Leng, M. J., Kender, S., Hesselbo, S. P., & Feist-Burkhardt, S. (2013). Isotopic and

776   palynological evidence for a new Early Jurassic environmental perturbation. *Palaeogeography,*

777   *Palaeoclimatology, Palaeoecology*, 374, 16 – 27. https://doi.org/10.1016/j.palaeo.2012.10.019

778   Robinson, S. A., Ruhl, M., Astley, D. L., Naafs, B. D. A., Farnsworth, A. J., Bown, P. R. et al. (2017).

779   Early Jurassic North AtlanXc sea-surface temperatures from TEX[86] palaeothermometry.

780   *Sedimentology*, 64(1), 215 – 230. https://doi.org/10.1111/sed.12321

781   Rubincam, D. P. (1994). Insolation in terms of Earth's orbital parameters. *Theoretical and applied*

782   *climatology*, 48, 195 – 202. https://doi.org/10.1007/BF00867049

783   Ruffell, A., McKinley, J. M. & Worden, R. H. (2002). Comparison of clay mineral stratigraphy to

784   other proxy palaeoclimate indicators in the Mesozoic of NW Europe. *Philosophical Transactions of*

785   *the Royal Society London A: Mathematical, Physical and Engineering Sciences*, 360, 675 – 693.

786   https://doi.org/10.1098/rsta.2001.0961

787   Ruhl, M., Hesselbo, S. P., Hinnov, L., Jenkyns, H. C., Xu, W., Riding, J. B., et al. (2016).

788   Astronomical constraints on the duration of the Early Jurassic Pliensbachian Stage and global climatic

789   fluctuations. *Earth and Planetary Science Letters*, 455, 149 – 165.

790   https://doi.org/10.1016/j.epsl.2016.08.038

791   Scott, A. C. (2000). The Pre-Quaternary history of fire. *Palaeogeography, Palaeoclimatology,*

792   *Palaeoecology*, 164(1- 4), 281 – 329. https://doi.org/10.1016/S0031-0182(00)00192-9

793   Scott, A. C., & Damblon, F. (2010). Charcoal: Taphonomy and significance in geology, botany and

794   archaeology. *Palaeogeography, Palaeoclimatology, Palaeoecology*, 291(1-2), 1 – 10.

795   https://doi.org/10.1016/j.palaeo.2010.03.044

796   Sellwood, B. W., & Valdes, P. J. (2008). Jurassic climates. *Proceedings of the Geologists'*

797   *Association*, 119(1), 5 – 17. https://doi.org/10.1016/S0016-7878(59)80068-7

798   Silva, R. L., Duarte, L. V., Wach, G. D., Ruhl, M., Sadki, D., Gómez, J. J. et al. (2021). An Early

799   Jurassic (Sinemurian–Toarcian) stratigraphic framework for the occurrence of organic matter

800   preservation intervals (OMPIs). *Earth-Science Reviews*, 221, 103780.

801   Slater, S. M., Twitchett, R. J., Danise, S., & Vajda, V. (2019). Substantial vegetation response to Early

802   Jurassic global warming with impacts on oceanic anoxia. *Nature Geoscience*, 12(6), 462 – 467.

803   https://doi.org/10.1038/s41561-019-0349-z

804   Steinthorsdottir, M., & Vajda, V. (2015). Early Jurassic (late Pliensbachian) CO2 concentrations

805   based on stomatal analysis of fossil conifer leaves from eastern Australia. *Gondwana Research*, 27(3),

806   932 – 939. https://doi.org/10.1016/j.gr.2013.08.021

807 Storm, M. S., Hesselbo, S. P., Jenkyns, H. C., Ruhl, M., Ullmann, C. V., Xu, W., et al. (2020). Orbital

808 pacing and secular evolution of the Early Jurassic carbon cycle. *Proceedings of the National Academy*

809 *of Sciences*, 117(8), 3974 – 3982. https://doi.org/10.1073/pnas.1912094117

810 The MathWorks Inc. (2021). MATLAB version: 9.11.0 (R2021b), Natick, Massachusetts: The

811 MathWorks Inc. https://www.mathworks.com

812 The MathWorks Inc. (2023). MATLAB version: 9.14.0 (R2023b), Natick, Massachusetts: The

813 MathWorks Inc. https://www.mathworks.com

814 Torsvik, T. H., & Cocks, L. R. M. (2017). Jurassic. In *Earth History and Palaeogeography*.

815 Cambridge: Cambridge University Press.

816 Trenberth, K. E., Fasullo, J., & Smith, L. (2005). Trends and variability in column-integrated

817 atmospheric water vapor. *Climate dynamics*, 24(7), 741 – 758. https://doi.org/10.1007/s00382-005-

818 0017-4

819 Ullmann, C. V., Szücs, D., Jiang, M., Hudson, A. J., & Hesselbo, S. P. (2022). Geochemistry of

820 macrofossil, bulk rock and secondary calcite in the Early Jurassic strata of the Llanbedr (Mochras

821 Farm) drill core, Cardigan Bay Basin, Wales, UK. *Journal of the Geological Society*, 179(1).

822 https://doi.org/10.1144/jgs2021-018

823 van de Schootbrugge, B., Bailey, T. R., Rosenthal, Y., Katz, M. E., Wright, J. D., Miller, K. G., et al.

824 (2005). Early Jurassic climate change and the radiation of organic-walled phytoplankton in the Tethys

825 Ocean. *Paleobiology*, 31(1), 73 – 97. https://doi.org/10.1666/0094-

826 8373(2005)031<0073:EJCCAT>2.0.CO;2

827 van der Werf, G. R., Randerson, J. T., Giglio, L., Collatz, G. J., Kasibhatla, P. S., & Arellano Jr, A. F.

828 (2006). Interannual variability in global biomass burning emissions from 1997 to 2004. *Atmospheric*

829 *Chemistry and Physics*, 6(11), 3423 – 3441. https://doi.org/10.5194/acp-6-3423-2006

830 Van Konijnenburg-Van Cibert, J. H. A. (2002). Ecology of some late Triassic to early Cretaceous

831 ferns in Eurasia. *Review of Palaeobotany and Palynology*, 119(1-2), 113 – 124.

832 https://doi.org/10.1016/S0034-6667(01)00132-4

833 Westerhold, T., Marwan, N., Drury, A. J., Liebrand, D., Agnini, C., Anagnostou, E. et al. (2020). An

834 astronomically dated record of Earth's climate and its predictability over the last 66 million years.

835 *Science*, 369(6509), 1383 – 1387. https://doi.org/10.1126/science.aba6853

836 Willes, K. & McElwain, J. (2014) The Evolution of Plants, Oxford University Press.